JPE 18-4-25

https://doi.org/10.6113/JPE.2018.18.4.1235
ISSN(Print): 1598-2092 / ISSN(Online): 2093-4718

Identification and Damping of Resonances in Inverter-based Microgrids

Morteza Afrasiabi* and Esmaeel Rokrok†

†,*Department of Electrical Engineering, Lorestan University, Khoramabad, Iran

Abstract

The application of shunt capacitor banks and underground cables typically induces resonance in power distribution systems. In this study, the propagation of resonance in a microgrid (MG) with inverter-based distributed generators (IBDGs) is investigated. If resonances are not properly damped, then the output current of the inverters may experience distortion via resonance propagation due to the adverse effect of resonances on MG power quality. This study presents a conceptual method for identifying resonances and related issues in multi-inverter systems. For this purpose, existing resonances are identified using modal impedance analysis. However, some resonances may be undetectable when this method is used. Thus, the resonances are investigated using the proposed method based on the frequency response of a closed-loop MG equivalent circuit. After analyzing resonance propagation in the MG, an effective virtual impedance damping method is used in the IBDG control system to damp the resonances. Results demonstrate the effectiveness of the proposed method in compensating for existing resonances.

Key words: Distributed Generation, Harmonic, Interface Inverter, Resonance, Virtual Impedance

I. INTRODUCTION

Distributed energy resources are generally connected to distribution systems via an interface inverter to deliver power and enhance network power quality. When an inverter-based distributed generator (IBDG) is connected to a stiff power system, the filter parameters of the inverter can be designed independently from its network parameters. Furthermore, low-voltage networks frequently have high impedance lines, and thus, coupling between IBDGs and networks must be considered. Accordingly, reciprocal impacts among all IBDGs and networks must be accounted for to identify resonances in multi-inverter systems.

Many studies have been conducted on the modeling of parallel inverters and the damping of resonances in microgrids (MGs). In [1], a simplified passive circuit model was presented to investigate resonances without the contribution of IBDGs. Reference [2] discussed the interaction of parallel inverters based on an open-loop transfer function matrix. However, this model cannot describe the transient behavior of MGs. Meanwhile, a method for damping resonance using an inductor–capacitor–inductor (LCL) filter was developed and presented in [3]. However, this method is sensitive to system parameter variations. In [4], [5], a double-loop line current control was applied to compensate for harmonics. However, double-loop control requires additional measurement systems. The virtual impedance compensation method (active damping) has been applied to stand-alone and grid-connected inverter applications [6]-[10]. The performance of virtual impedance control can be less sensitive to system parameter variations.

In [11], a method was applied to identify and actively damp resonances in parallel inverters. However, this method is only applicable to multi-parallel inverters that can be connected to one bus. In [12], an active damper with a series LC filter was presented to suppress resonances in an AC MG with IBDGs. Compared with an active power filter for mitigating low-frequency harmonics, the proposed damper damps resonances at higher frequencies. Reference [13] introduced different active damping approaches based on high-order harmonic elimination for grid-connected inverters with LCL filters. The use of resistor–capacitor impedance in the output of parallel inverters was presented in [14] to reduce circulating currents and damp high-frequency resonances among inverters. A new active damping control strategy that introduced a positive capacitor or a negative inductor as

Manuscript received Nov. 3, 2017; accepted Feb. 20, 2018
Recommended for publication by Associate Editor Jongbok Baek.
†Corresponding Author: rokrok.e@lu.ac.ir
Tel: +98- 66-33120097, Fax: +98- 66-33120106, Lorestan University
*Dept. of Electrical Engineering, Lorestan University, Iran

virtual impedance in doubly-fed induction generators was demonstrated in [15]. Most of the aforementioned methods have been successfully applied to mitigate resonances; however, the effectiveness of these methods depends on the exact identification of network resonances. Thus, good power quality can be guaranteed if all the resonances of an MG are accurately identified and damped.

The current study models an inverter-based MG to identify resonances and resonance frequencies. In the presented approach, the closed-loop MG equivalent circuit is determined according to the network admittance model. Then, the resonance frequencies are determined based on frequency response analysis. The impact of all the elements can be considered in the presented approach due to its flexibility. Subsequently, the MG resonances are examined via modal impedance analysis, and the relation of this approach to the proposed method is evaluated. Consequently, an effective active damping method is used in an IBDG control system to damp the identified resonances.

The rest of the paper is organized as follows. Section II discusses the modeling of MG components. Section III analyzes MG resonances. Section IV investigates the principle of the resonance damping strategy. Section V simulates a sample MG. Section VI draws the conclusions of the study.

II. IBDG MG

Fig. 1 shows the single-line diagram of the proposed three-phase balanced MG. This MG consists of two current control inverters, which are used to supply the predefined powers to the MG in grid-connected operation mode. L_f, L_g, and C_f are the inverter side inductance, network side inductance, and filter capacitor, respectively. Z_{li}, Z_{grid}, and Z_{load} are the line, grid, and load impedances, respectively.

A. Inverter Modeling

Fig. 2(a) shows the control system of the current control inverter. The inverter output has an LCL filter, and the inverter current control loop includes a proportional resonant (PR) controller that is designed in a stationary reference frame. A phase-locked loop is used to synchronize the current control inverter with the MG. A pulse-width modulation (PWM) converter is linearized around the operation point of the system, and the relation among the inverter output current, reference current, and output voltage can be obtained as follows:

$$I_o(S) = G_{cc}(S).I^*(s) - Y_{oc}(S).V_o(s). \quad (1)$$

Equation (1) represents the Norton equivalent circuit of the current control inverter, in which $G_{cc}(S)$, $Y_{oc}(S)$, and $I^*(s)$ denote the closed-loop transfer current function, output admittance, and reference current of the current control inverter, respectively. $G_{cc}(S)$ and $Y_{oc}(S)$ can be computed using Fig. 2(b) and Masson's formula as follows:

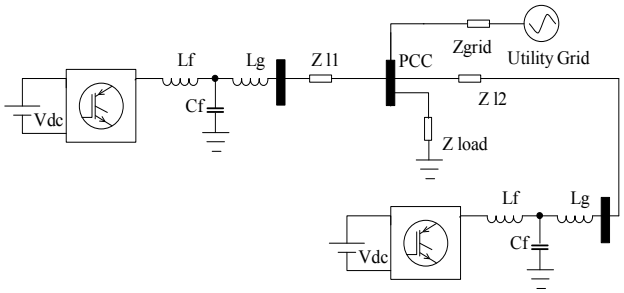

Fig. 1. Three-phase balanced MG.

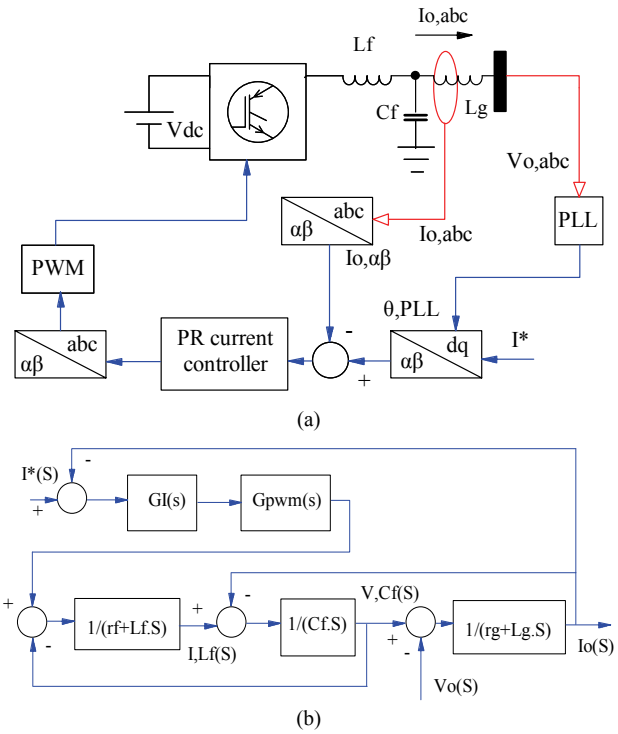

Fig. 2. Per-phase equivalent model of the inverter: (a) Schematic of the control system, (b) Block diagram of the linearized system.

$$G_{cc}(S) = \frac{G_I(s).G_{pwm}(S)}{C_f.s(r_f+s.L_f)(r_g+s.L_g)+(r_f+s.L_f)+(r_g+s.L_g)+G_I(s).G_{pwm}(S)}, \quad (2)$$

$$Y_{oc}(S) = \frac{C_f.s(r_f+s.L_f)+1}{C_f.s(r_f+s.L_f)(r_g+s.L_g)+(r_f+s.L_f)+\cdots}, \quad (3)$$

where r_f and r_g are the internal resistance of the filter inductances, and $G_I(S)$ is the PR transfer function of the current controller that is written as

$$G_I(s) = K_{pi} + \sum_{K=1,5,\ldots,19} \frac{K_{ri}.s}{s^2+(k.\omega^*)^2}, \quad (4)$$

where K_{pi} and K_{ri} are the proportional and kth harmonic (including the fundamental component as the first harmonic) resonant coefficients of the current controller, and ω^* represents the fundamental frequency. The transfer function of the PWM converter is considered

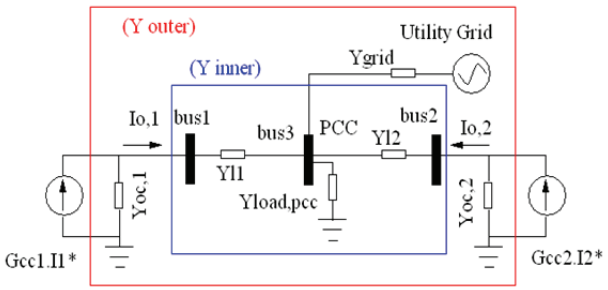

Fig. 3. Per-phase equivalent circuit of the MG.

$$G_{pwm}(s) = \frac{1}{1+1.5.T_s.s}, \tag{5}$$

where T_s is the converter switching period.

B. Closed-loop Equivalent Circuit of the MG

Fig. 3 illustrates the equivalent circuit of the MG in which all resources are substituted with the Norton model for simplicity. The MG lines and loads are modeled with constant impedances. First, the admittance matrix is constructed for the outer zone when the MG is connected to the upstream network. In this case, the output impedances of the IBDGs are considered in the admittance matrix of the MG, and the voltage control inverter is out of service. Therefore, the admittance matrix is

$$\begin{bmatrix} G_{cc,1}.{I_1}^* \\ G_{cc,2}.{I_2}^* \\ Y_{grid}.{V_{grid}}^* \end{bmatrix} = [Y_{outer}].\begin{bmatrix} V_1 \\ V_2 \\ V_3 \end{bmatrix}, \tag{6}$$

where $[Y_{outer}]$ is the outer admittance matrix (outer area) wherein the inverter's output impedances are considered. ${I_i}^*$, V_i, ${V_{grid}}^*$, and Y_{grid} are the reference current of the i_{th} inverter, voltage of the i_{th} bus, grid voltage, and grid admittance, respectively.

$$[Y_{outer}]= \tag{7}$$

$$\begin{bmatrix} Y_{oc,1}+Y_{l,1} & 0 & -Y_{l,1} \\ 0 & Y_{oc,2}+Y_{l,2} & -Y_{l,2} \\ -Y_{l,1} & -Y_{l,2} & Y_{grid}+Y_{l,1}+Y_{load,pcc}+\cdots \end{bmatrix},$$

where $Y_{l,i}$ is the line admittance and $Y_{load,pcc}$ is the load admittance at the point of common coupling (PCC).

$$[Z_{outer}] = [Y_{outer}]^{-1}, \tag{8}$$

$$\begin{bmatrix} V_1 \\ V_2 \\ V_3 \end{bmatrix} = [Z_{outer}].\begin{bmatrix} G_{cc,1}.{I_1}^* \\ G_{cc,2}.{I_2}^* \\ Y_{grid}.{V_{grid}}^* \end{bmatrix}. \tag{9}$$

The inner zone admittance should be used to calculate the output current of IBDGs. In this case, the IBDG output impedances will not be included in the admittance matrix. Therefore,

$$\begin{bmatrix} I_{0,1} \\ I_{0,2} \\ I_{0,3} \end{bmatrix}=[Y_{inner}].\begin{bmatrix} V_1 \\ V_2 \\ V_3 \end{bmatrix}, \tag{10}$$

where $[Y_{inner}]$ and $I_{o,i}$ are the inner zone admittance matrix and the output current of each IBDG, respectively.

$$[Y_{inner}]=\begin{bmatrix} Y_{l,1} & 0 & -Y_{l,1} \\ 0 & Y_{l,2} & -Y_{l,2} \\ -Y_{l,1} & -Y_{l,2} & Y_{l,1}+Y_{l,2}+Y_{load,pcc} \end{bmatrix}, \tag{11}$$

$$\begin{bmatrix} I_{0,1} \\ I_{0,2} \\ I_{0,3} \end{bmatrix}=[Y_{inner}].[Z_{outer}].\begin{bmatrix} G_{cc,1}.{I_1}^* \\ G_{cc,2}.{I_2}^* \\ Y_{grid}.{V_{grid}}^* \end{bmatrix}, \tag{12}$$

$$[Y_{inner}].[Z_{outer}] = [G] = \begin{bmatrix} G_{11} & G_{12} & G_{13} \\ G_{21} & G_{22} & G_{23} \\ G_{31} & G_{32} & G_{33} \end{bmatrix}, \tag{13}$$

where $[G]$ is the network transfer function matrix. To calculate the output current of each IBDG (e.g., IBDG1), their current can be extended as follows:

$$I_{o,1} = G_{11}.G_{cc,1}.{I_1}^* + G_{12}.G_{cc,2}.{I_2}^* + G_{13}.Y_{grid}.{V_{grid}}^*. \tag{14}$$

The relation between IBDG1 current and ${I_1}^*$, ${I_2}^*$, and ${V_{grid}}^*$ is as follows:

$$\frac{I_{0,1}}{{I_1}^*} = G_{11}.G_{cc,1}\left|{V_{grid}}^*, {I_2}^* = 0, \right. \tag{15}$$

$$\frac{I_{0,1}}{{I_2}^*} = G_{12}.G_{cc,2}\left|{V_{grid}}^*, {I_1}^* = 0, \right. \tag{16}$$

$$\frac{I_{0,1}}{{V_{grid}}^*} = G_{13}.Y_{grid}\left|{I_1}^*, {I_2}^* = 0. \right. \tag{17}$$

When Equation (14) is considered, the output current of each inverter depends on three terms. Each term can contain resonances. The first term that makes up internal resonance represents the dependency of the i_{th} inverter output current to its own reference change. The second term shows parallel resonance between IBDGs and is generated by the reference change in other inverters. The third term indicates the interaction between the i_{th} inverter output current and grid voltage. This type of resonance can be excited during voltage distortion. Therefore, MG resonances can be understood by observing the frequency response plot of the aforementioned transfer functions.

III. Analyzing Network Resonances

To demonstrate the performance of the aforementioned method in identifying MG resonances, MG resonances are analyzed using the proposed method (the closed-loop MG equivalent circuit) and the modal impedance method proposed in [4]. Then, the differences between the two methods are determined. The modal impedance matrix $[Z_m]$ is calculated using Equations (18) to (21). In accordance with these equations, if the input current vector [I] is always set to 1 p.u., then the high voltage vector $[V]$ values are

associated with the singularity of the admittance matrix $[Y_{outer}]$. The singularity of the $[Y_{outer}]$ matrix can be observed when one of its eigenvalue is close to zero.

$$[V] = [Z_{outer}].[I] = [Y_{outer}]^{-1}.[I], \quad (18)$$

$$[Y_{outer}] = [L][\Lambda][T], \quad (19)$$

$$[V] = [L][\Lambda]^{-1}[T].[I], \quad (20)$$

$$[Z_m] = [\Lambda]^{-1}, \quad (21)$$

where $[T]$, $[L]$, and $[\Lambda]$ are the matrices constructed from the right and left eigenvectors and the diagonal matrix composed of the eigenvalues of the admittance matrix. Evidently, if the eigenvalues of the $[\Lambda]$ matrix tend to be small, then the modal impedances of the $[Z_m]$ matrix move toward the large values and cause the propagation of parallel resonances. The modal impedance approach is constantly a powerful instrument for detecting resonances in power systems. However, resonance frequencies may not be detected in this method because modal impedance analysis is a passive approach. Therefore, the closed-loop equivalent circuit method and modal impedance analysis are used simultaneously in this study to detect system resonances.

A. MG Resonances in Grid-connected Mode

The resonances in the IBDG1 output current are investigated in this section. MG resonances are investigated by considering the parameters of the control system and power circuit listed in Table 1. Fig. 4 illustrates the Bode plot of the transfer function $\frac{I_{0,1}}{I_1^*}$ and modal impedance components of the aforementioned system (Fig. 3). In this case, line impedances are neglected, and bus 3 is connected to the grid. As shown in Fig. 4, when one inverter is connected to the network, only one resonance frequency occurs in the MG due to the inverter output filter capacitor. This resonance frequency matches the resonance frequency in the modal impedance diagram.

As shown in the modal impedance diagram in different statuses (multi-inverter), only Z_{m3} is excited, whereas Z_{m1} and Z_{m2} can be neglected. Z_{m3} is also moved to low frequencies by increasing the number of inverters (new inverters are added to bus 2). The frequency response diagram of IBDG1 includes two pick points. The low-frequency pick point is identical to the modal impedance diagram due to the increased number of parallel inverters. This point is moved to low frequencies by increasing the number of inverters. The second peak point is constant and is related to the inverter's closed-loop transfer function G_{cc}. The second peak point is unavailable in the modal impedance diagram. The discussed resonances, called internal resonances, are typically transient resonances that can be excited during the reference change of IBDGs.

The other IBDGs can also cause the second type of resonance

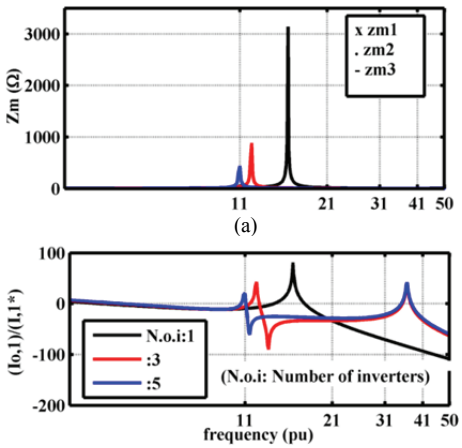

Fig. 4. Internal resonances of IBDG1: (a) Modal impedance plot, (b) Magnitude Bode plot for the transfer function $\frac{I_{0,1}}{I_1^*}$.

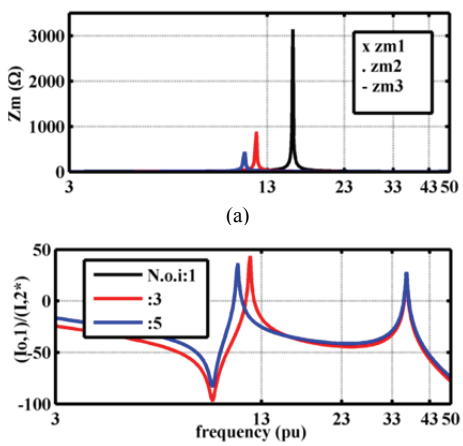

Fig. 5. Parallel resonances between IBDG1 and IBDG2: (a) Modal impedance plot, (b) Magnitude Bode plot for the transfer function $\frac{I_{0,1}}{I_2^*}$.

in the IBDG1 output current. These resonances, which are generated among IBDG currents, are presented in Fig. 5. In this case, the frequency response of transfer function $\frac{I_{0,1}}{I_2^*}$ has two peak points in the diagram. The high frequency point is associated with the closed-loop transfer function of IBDGs, whereas the low frequency point is related to the inverter's output impedances.

When the MG is connected to the upstream grid, the harmonics in the grid voltage can distort the output current of the IBDGs (Fig. 6).

These propagated resonances are the third type of resonances in the MG. In this situation, the $\frac{I_{0,1}}{V_{grid}^*}$ frequency response plot has only one peak point, which is identical to the maximum point of the modal impedance plot. The peak point moves to low frequencies with an increase in the number of parallel IBDGs. The grid voltage typically has

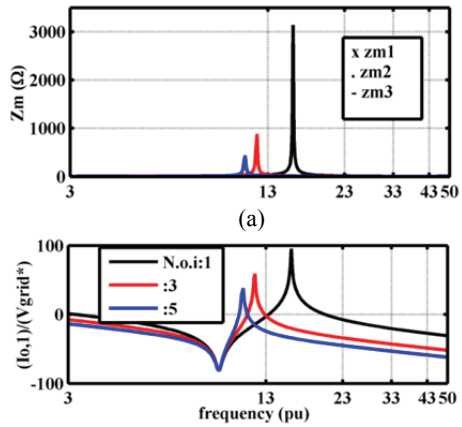

(a)

(b)

Fig. 6. Parallel resonances between the grid and IBDG1: (a) Modal impedance plot, (b) Magnitude Bode plot for the transfer function $\frac{I_{0,1}}{V_{grid}{}^{*}}$.

low-order harmonics in the steady state situation. When the number of parallel IBDGs increases in the MG, the resonance frequencies can possibly get close to the grid harmonic frequencies. That is, the low-order harmonics of the grid voltage may excite MG resonances. The internal and parallel resonances among IBDGs are typically excited by transient states. However, the third type of resonance can possibly occur under steady state condition due to the low-order harmonics in the grid voltage.

B. Effect of Capacitor and Line Impedances

The power factor correction capacitor and line impedances affect network resonances. To investigate the effect of capacitors, only IBDG1 is assumed to be in service, whereas the other inverters are disconnected and bus 3 is connected to the main grid. Two maximum points are created in the modal impedance diagram of Z_{m3} by adding a 40 μF capacitor to bus 1 (Fig. 7).

When the second capacitor (with the same capacity) is added to bus 2 by neglecting the line impedances, the generated state is the same as that in the previous scenario but with twice the capacitor capacity. The frequencies of the two peak points move away from each other by increasing the number of capacitors. When the effect of line impedance on the resonance analysis is considered, a new mode is created in the network as shown in Fig. 8, and previous modes move to lower or higher frequencies by adding each capacitor. In case low-order harmonics occur in the network voltage, the modes that move to lower frequencies may produce permanent resonances.

C. Grid Impedance Impact

As shown in Fig. 9, the magnitude of the modal impedance peak point is decreased drastically by reducing the grid inductance L_{grid} and the mode tends toward higher frequencies. The IBDGs can be considered independent from

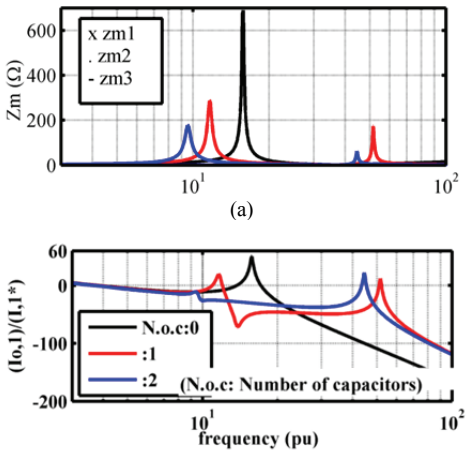

(a)

(b)

Fig. 7. Internal resonances with power factor correction capacitors: (a) Modal impedance plot, (b) Magnitude Bode plot for the transfer function $\frac{I_{0,1}}{I_1{}^{*}}$.

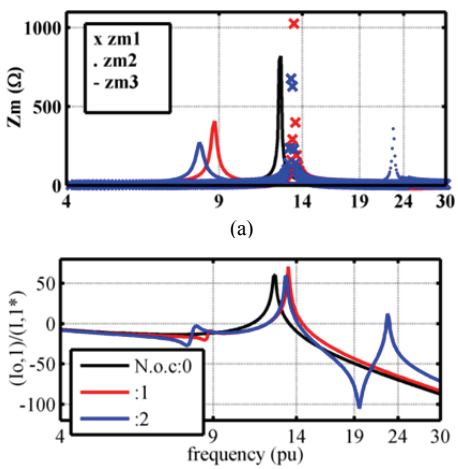

(a)

(b)

Fig. 8. Internal resonances with power factor correction capacitors and that consider line impedances: (a) Modal impedance plot, (b) Magnitude Bode plot for the transfer function $\frac{I_{0,1}}{I_1{}^{*}}$.

one another when the MG is connected to the upstream grid via a low impedance line (stiff grid).

However, when a high impedance line (weak grid) exists, the dynamic behavior of the IBDGs is dependent on one another and grid impedance should be considered in network analysis. The important points of analysis can be listed as follows.

- The reference change of IBDGs creates the transient resonances in the output current of the inverters.
- Each power factor correction capacitor or filter connected to a separate bus creates a new resonance mode in the network.
- Only one resonance is created when filters or capacitors are connected to one bus, and its frequency changes based on capacitor value.

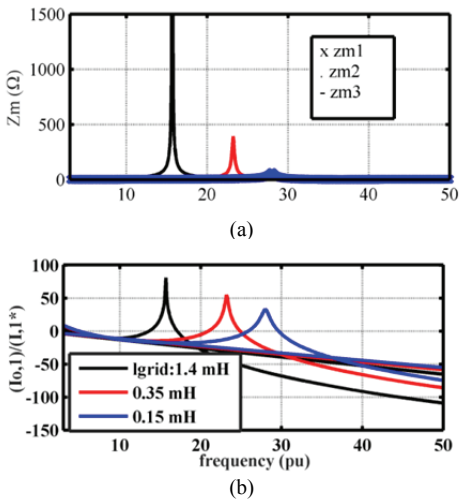

Fig. 9. Internal resonances of grid impedances with different values: (a) Modal impedance plot, (b) Magnitude Bode plot for the transfer function $\frac{I_{0,1}}{I_1^*}$.

- Some resonances tend toward low frequencies by increasing line inductances.
- The dependence of IBDGs on one another and the magnitude of network resonances are reduced with decreasing grid inductance.

On the basis of these points, if network resonances are not properly damped, then the quality of IBDG output current and network voltage may experience a major distortion.

IV. Resonance Damping Strategy

Reference [16] suggested a method for the active compensation of distortions in a single inverter system. In this method, the application of parallel inverters is not considered. The lag-and-lead compensation method in [2] is applicable to parallel inverters but highly dependent on network parameters and uncertainties. Furthermore, the virtual impedance approach in grid-connected inverters was used in [9–11] and [17, 18], which show that the virtual impedance method is less sensitive to a change in network parameters. Moreover, no power loss occurs because the resistor is not physically connected to the network. Therefore, the virtual resistance method is used to mitigate network resonances in the succeeding sections of this paper.

A. Damping Scheme

Fig. 10 shows the control current inverter with a virtual damping resistor. The output voltage is transformed to the (synchronous) dq reference frame, and voltage distortion is separated by using a high-pass filter.

Then, voltage distortion is transformed to the (stationary) αβ reference frame. Afterward, voltage distortion is damped by the R_v resistor, which exerts the same effect on all the harmonic components. The gain of the damping control loop

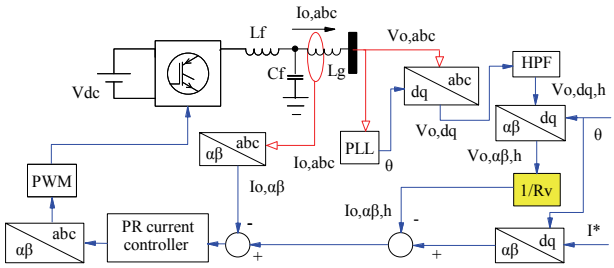

Fig. 10. Per-phase equivalent model of the current control inverter with a virtual damping resistor.

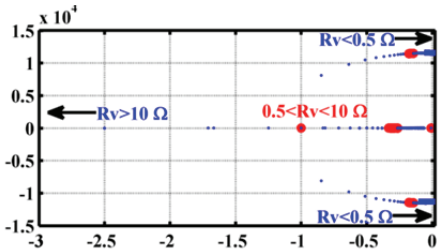

Fig. 11. Root map of an inverter system with different damping resistances (R_v changes from 40 Ω to 0.2 Ω).

is considered $1/R_v$. In the fundamental frequency, this damping resistor behaves similarly to an infinite resistor and exerts no impact on the fundamental component.

B. Stability Analysis and Design Guidelines

To achieve a mathematical approach for computing the damping resistor by considering the inverter Norton equivalent circuit (Equation (1)) and regardless of the resistances and simplification, the reduced second-order system is obtained as [11]

$$I_o(S) = \frac{\frac{1}{C_f(L_f+L_g)}}{S^2+\left(\frac{1}{C_f.R_v}\right).S+\frac{1}{C_f(L_f+L_g)}}.I^*(s) - \frac{S^2+\left(\frac{1}{C_f.R_v}\right)}{S^2+\left(\frac{1}{C_f.R_v}\right).S+\frac{1}{C_f(L_f+L_g)}}.V_o(s). \quad (22)$$

The damping ratio (σ) is achieved as

$$\sigma = \frac{1}{2R_v}\sqrt{\frac{L_f+L_g}{C_f}}. \quad (23)$$

The damping resistance can be obtained by considering the favorable damping ratio.

The stability analysis of the inverter system is also investigated. Fig. 11 shows the root map of the inverter system with different virtual damping resistances. The circuit parameters of the system are selected to be the same as those in the simulation, which are listed in Table I.

As shown in Fig. 11, when R_v is set as 0.5 Ω, the system has a conjugate pole pair around the imaginary axis, which illustrates a decrease in system stability margin and weak damping characteristic. Furthermore, the conjugate pole pair

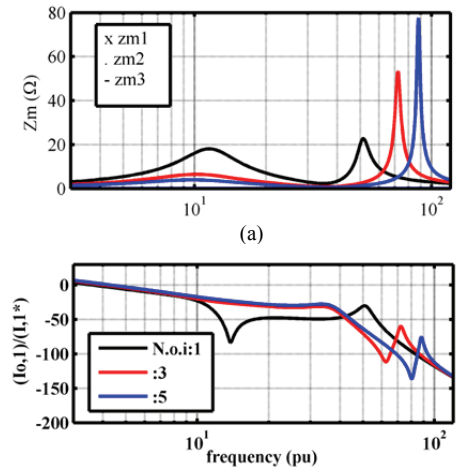

Fig. 12. Internal resonances with a virtual damping resistor: (a) Modal impedance plot, (b) Magnitude Bode plot for the transfer function $\frac{I_{0,1}}{I_1^*}$.

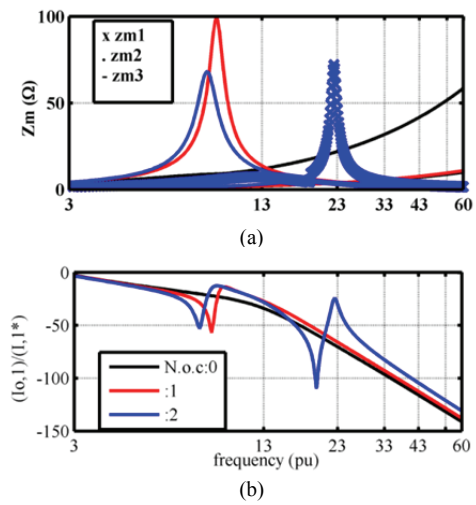

Fig. 13. Internal resonances with power factor correction capacitors and the impact of virtual damping resistors: (a) Modal impedance plot, (b) Magnitude Bode plot for the transfer function $\frac{I_{0,1}}{I_1^*}$.

moves toward the right side of the imaginary axis with a small damping resistance. When R_v is reduced to 0.2 Ω, the conjugate pole pair passes the imaginary axis and the system becomes unstable. Fig. 11 also shows that when R_v changes from 6 Ω to 10 Ω, the position variation of the poles are not highly evident. However, when R_v changes from 10 Ω to 40 Ω, the positions of the poles exhibit considerable changes. From these discussions, the appropriate virtual damping resistance for inverters can be achieved.

C. Damping Effect on Resonances

Fig. 12 shows the impact of a damping virtual resistor on modal impedance and the closed-loop transfer function $\frac{I_{0,1}}{I_1^*}$ when the virtual resistor is set as 9 Ω.

TABLE I
PARAMETERS OF THE CONTROL AND ELECTRICAL POWER SYSTEM

Symbol	Parameter	Value	Unit
E	Grid voltage amplitude	311	V
V_{dc}	DC link voltage	650	V
$\omega*$	Grid frequency	314	Rad/s
$Z_{load,pcc}$	Load impedance	6+j3.5	Ω
L_g, L_f	Filter inductance	0.2,1.8	mH
F_s	Switching frequency	10	kHZ
Z_{l1}, Z_{l2}, Z_{grid}	Line inductance	j0.62, j0.62,j0.3	Ω
R_v	Virtual resistance	9	Ω
C_f	Filter capacitor	25	μF
k_{pi}, k_{ri}	Controller coefficient	1,100	W/rd

The resonance magnitude is reduced from 30 dB to −5 dB according to Fig. 12 and the comparison of the resonance peak value with the uncompensated case (Fig. 4). When the power factor correction capacitors and line impedances are considered, the virtual resistors affect network resonances. As shown in Fig. 13, some modes tend toward infinite frequencies and the magnitudes of other modes also decrease considerably compared with the uncompensated case (Fig. 8). This type of compensation significantly affects the damping of MG resonances.

V. RESULTS

The results of the two cases are presented in this section. In Case 1, the experimental and simulation results of the mitigation of internal and parallel resonances are presented in the MG. In Case 2, only the simulation results are presented for the damping of resonances between the grid and the MG because of the limit in the number of inverters.

The electrical power system shown in Fig. 3, which comprises an MG and a utility grid, is considered the test system to validate the proposed method. The MG works at 220 V and 50 Hz. The parameters of the MG and control system are presented in Table I. Parallel inverters have similar parameters.

A. Case 1: Internal and Parallel Resonances of the MG

In the experiment, DGs are controlled with a DS1103 dSPACE controller card. dSPACE ControlDesk is adopted as the user interface. Simulations are performed using MATLAB Simulink software., All the control parameters are the same for the simulation and the experiment to provide a fair comparison. As shown in Fig. 3, two inverters (connected to buses 1 and 2) supply the PCC load in this case, whereas bus 3 is connected to the grid. First, a step change occurs in the current reference signal of inverter 1 at t = 0.2 s, and the inverter output current increases from 15 A to 22 A (current

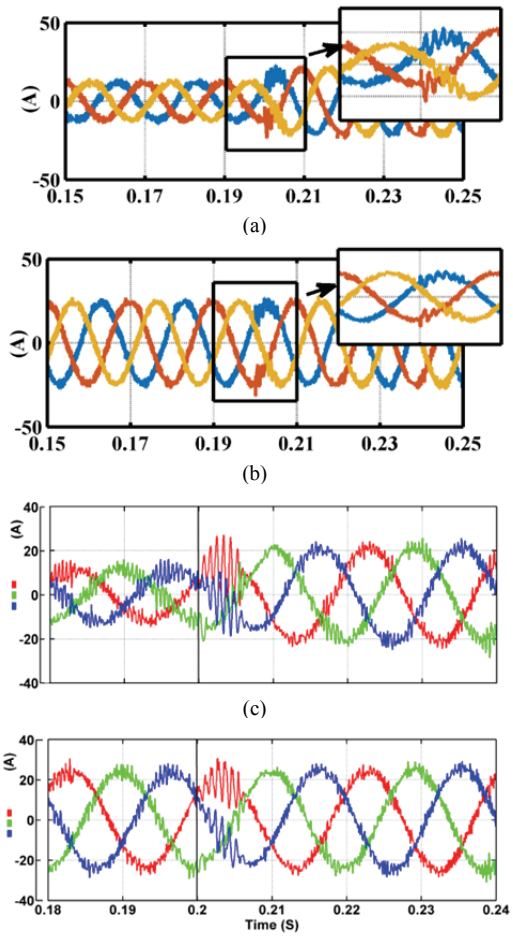

Fig. 14. Output currents before damping: (a) Inverter 1 (simulation), (b) Inverter 2 (simulation), (c) Inverter 1 (experiment), (d) Inverter 2 (experiment).

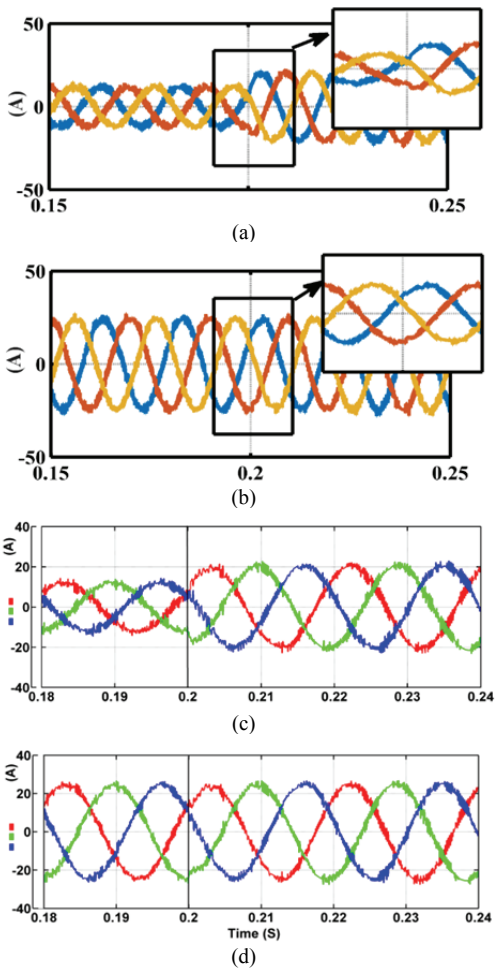

Fig. 15. Output currents after damping: (a) Inverter 1 (simulation), (b) Inverter 2 (simulation), (c) Inverter 1 (experiment), (d) Inverter 2 (experiment).

peak), which is observable in Figs. 14(a) and 14(c). The reference of inverter 2 is fixed at 23 A. During this change, transient oscillation occurs in the line current and the amount of total harmonic distortion (THD) of inverter 1 output current increases to 25%. This variation in the output current of inverter 1 affects inverter 2, which has a constant reference (parallel resonance among inverters), and distorts its output current. This result is illustrated in Figs. 14(b) and 14(d).

Virtual damping resistors are used in the inverter control system to reduce existing resonances. Figs. 15(a) and 15(c) show that the amount of distortion in the inverter 1 output current decreases due to the virtual damping resistor. The THD amount of IBDG1 output current at the moment of reference change is decreased to 5% compared with the previous case (Figs. 14(a) and 14(c)). A decrease in oscillations through the use of a damping resistor in the output current of inverter 2 is also shown in Figs. 15(b) and 15(d).

The harmonics in the line current can distort PCC voltage. As shown in Fig. 16(a), PCC voltage has high order harmonics before the use of virtual resistors.

Fig. 16(b) shows that activating the virtual resistors leads to a significant reduction in PCC voltage THD in steady state. Voltage distortion is also mitigated effectively at the moment of switching compared with that in the uncompensated state. Finally, improvement in voltage quality can be observed in the waveforms.

B. Case 2: Induced Resonances of the Grid

To investigate resonance under steady state condition, 10% of the 11th harmonic is assumed to be added to the grid voltage and the MG operates with five inverters (one inverter is connected to bus 1 and four inverters are connected to bus 2).

When five parallel inverters with the same specifications are included in the MG (according to Fig. 6), resonance occurs and inverter output currents are distorted (Fig. 17(a)) because network resonance frequency is close to the 11_{th} harmonic frequency. After disconnecting bus 2 at t = 0.2 s, the four inverters connected to this bus are separated from the network, and resonance frequency increases to the upper value. In this case, the output current distortion of inverter 1 is improved considerably. The improved performance with

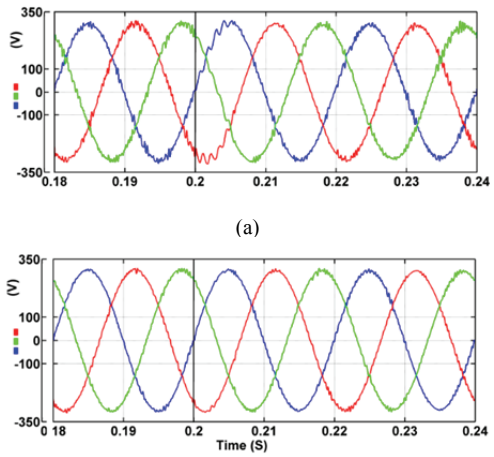

(a)

(b)

Fig. 16. PCC voltages: (a) PCC voltages before damping (experiment), (b) PCC voltages after damping (experiment).

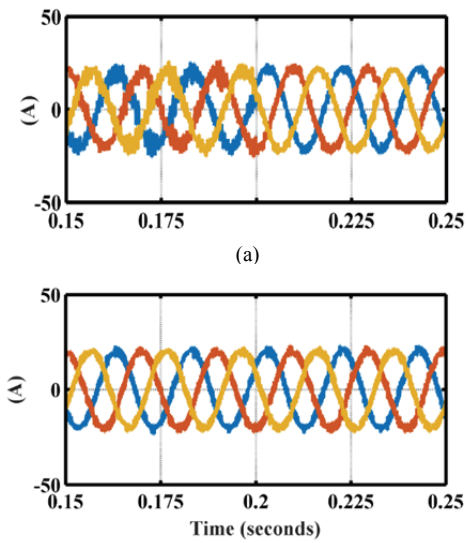

(a)

(b)

Fig. 17. Output currents: (a) Output currents of inverter 1 without damping (simulation), (b) Output currents of inverter 1 with damping (simulation).

active damping is also illustrated in Fig. 17(b). As shown in the figure, the output current of inverter 1 with a damping resistor (parallel with the other inverters) exhibits no distortion compared with the previous case (Fig. 17(a)).

VI. Conclusions

In this study, different types of resonance in an inverter-based MG are investigated. After analyzing the closed-loop MG equivalent circuit, the resonances and resonance frequencies are identified using two methods. When a simple model with a single inverter connected to the network is considered, multiple inverter analysis will not be sufficiently accurate. Moreover, parallel inverters with multiple resonances may cause transient or steady state distortions. To solve resonance problems, an effective method for damping resonances is used. The results showed that the proposed method can effectively reduce the multiple resonances of a network.

References

[1] J. H. R. Enslin and P. J. M. Heskes, "Harmonic interaction between a large number of distributed power inverters and the distributed network," *IEEE Trans. Power Electron.*, Vol. 19, No. 6, pp. 1586-1593, Nov. 2004.

[2] J. Agorreta, M. Borrega, J. Lopez, and L. Marroyo, "Modeling and control of N paralleled grid-connected inverters with LCL filters coupled due to grid impedance in PV plants," *IEEE Trans. Ind. Electron*, Vol. 26, No. 3, pp. 780-780, Mar. 2011.

[3] M. H. Bierhoff and F. W. Fuchs, "Active damping for three-phase PWM rectifiers with high-order line-side filters," *IEEE Trans. Ind. Electron*, Vol. 56, No. 2, pp. 371-379, Feb. 2010.

[4] M. Munir, Y. W. Li, and H. Tian, "Improved residential distribution system harmonic compensation scheme using power electronics interfaced DGs," *IEEE Trans. Smart Grid*, Vol. 7, No. 3, pp. 1191-1203, May 2016.

[5] M. Munir and Y.W. Li, "Residential distribution system harmonic compensation using pv interfacing inverter," *IEEE Trans. on Smart Grid*, Vol. 4, No. 2, pp. 816-827, Jun. 2013.

[6] J. He, Y. W. Li, D. Bosnjak, and B. Harris, "Investigation and resonances damping of multiple PV inverters," in *Conf. Rec. IEEE Annu. Appl. Power Electron.*, pp. 246-253, 2012.

[7] J. He and Y.W. Li, "Generalized closed-loop control (GCC) schemes with embedded virtual impedances for voltage source converters with LC or LCL filters," *IEEE Trans. Power Electron*, Vol. 27, No. 4, pp. 1850-1861, Apr. 2012.

[8] J. He, Y. W. Li, R. Wang, and C. Zhang, "Analysis and mitigation of resonance propagation in grid-connected and islanding MGs," *IEEE Trans. Energy Convers.*, Vol. 30, No. 1, pp. 70-81, Mar. 2015.

[9] Z. Chen, Y. Chen, J. M. Guerrero, H. Kuang, Y. Huang, L. Zhou, and A. Luo, "Generalized coupling resonance modeling, analysis, and active damping of multi-parallel inverters in MG operating in grid-connected mode," *Power Syst. Clean Energy*, Vol. 4, No. 1, pp. 63-75, 2016.

[10] Y. Han, P. Shen, and J. M. Guerrero, "Stationary frame current control evaluations for three-phase grid-connected inverters with pvr-based active damped LCL filters," *J. Power Electron.*, Vol. 16, No. 1, pp. 297-309, Jan. 2016.

[11] J. He, Y.W. Li, D. Bosnjak, and B. Harris, "Investigation and active damping of multiple resonances in a parallel inverter-based MG," *IEEE Trans. Power Electronics*, Vol. 28, No. 1, pp. 234-246, Jan. 2013.

[12] X. Wang, Y. Pang, P. C. Loh, and F. Blaabjerg, "A series-LC-filtered active damper with grid disturbance rejection for ac power-electronics-based power systems," *IEEE Trans. Power Electron.*, Vol. 30, No. 8, pp. 4037-4041, Aug. 2015.

[13] I. Lorzadeh, M. S. Firoozabadi, H. Askarian Abyaneh, and J. M. Guerrero, "Active damping techniques for LCL-filtered inverters-based MGs," *Proc. of the 10th IEEE International Symposium on Diagnostics for Electrical Machines, Power Electronics and Drives (SDEMPED)*, pp.

408-414, 2015.
[14] Y. Chen, J. M. Guerrero, Z. Shuai, Z. Chen, L. Zhou, and A. Luo, "Fast reactive power sharing, circulating current and resonance suppression for parallel inverters using resistive-capacitive output impedance," *IEEE Trans. Power Electron.*, Vol. 31, No. 8, pp. 5524-5537, Aug. 2016.
[15] Y. Song, X. Wang, and F. Blaabjerg, "High frequency resonance damping of DFIG based wind power system under weak network," *IEEE Trans. Power Electron.*, Vol. 32, No. 3, pp. 1927-1940, Mar. 2017.
[16] K. H. Ahmed, A. M. Massoud, S. J. Finney, and B. W. Williams, "A modified stationary reference frame-based predictive current control with zero steady-state error for LCL coupled inverter-based distributed generation systems," *IEEE Trans. Ind. Electron.*, Vol. 58, No. 4, pp. 1359-1370, Apr. 2011.
[17] F. Wang, J. L. Duarte, M. A. M. Hendrix, and P. F. Ribeiro, "Modeling and analysis of grid harmonic distortion impact of aggregated DG inverters," *IEEE Trans. Power Electron.*, Vol. 26, No. 3, pp. 786-797, Mar. 2011.
[18] W. Zhao and G. Chen, "Comparison of active and passive damping methods for application in high power active power filter with LCL-filter," in *Conf. Rec. IEEE Int. Conf. Sustainable Power Generation Supply*, pp. 1-6, 2010.

Morteza Afrasiabi was born in Azna, Iran in 1979. He obtained his M.Sc. in Power Electrical Engineering from Tafresh University, Iran in 2011. He is currently a Ph.D. student in the Electrical Engineering Department of Lorestan University, Khoramabad, Iran. His main research interests include power quality in distribution systems and microgrids.

Esmaeel Rokrok was born in Khoramabad, Iran in 1972. He obtained his B.Sc., M.Sc., and Ph.D. in Electrical Engineering from Isfahan University of Technology in 1985, 1997, and 2010, respectively. He is an assistant professor in the Department of Electrical Engineering, Lorestan University. His major research interests include power system control and dynamics, dispersed generation, microgrids, and robust control.